# Journal of Materials Chemistry A

Accepted Manuscript






ROYAL SOCIETY OF CHEMISTRY

www.rsc.org/materialsA

Journal Name

RSCPublishing

ARTICLE

# Oxygen Storage Capacity of $Sr_3Fe_2O_{7-\delta}$ Having High Structural Stability

Cite this: DOI: 10.1039/xoxxoooooox

Kosuke Beppu,[a] Saburo Hosokawa,[ab*] Kentaro Teramura[abc] and Tsunehiro Tanaka[ab*]

Received ooth January 2012,
Accepted ooth January 2012

DOI: 10.1039/xoxxoooooox

www.rsc.org/

The present study proves that $Sr_3Fe_2O_{6.75}$ has high performance of oxygen storage capacity as well as high structural stability under severe reduction conditions. The $H_2$ reduction of $Sr_3Fe_2O_{6.75}$ at 1223 K results in the formation of $Sr_3Fe_2O_6$, whereas $SrFeO_{2.84}$ easily decomposes to $Sr_3Fe_2O_6$ and Fe metal by the same treatment. The structural framework of $Sr_3Fe_2O_{6.75}$ is identical with that of $Sr_3Fe_2O_6$ bearing the space group of *I*4/*mmm*. In the crystal structure of $Sr_3Fe_2O_{6.75}$, three oxygen sites (8*g*, 4*e* and 2*a*) exist. Among those, only oxygen ions in 2*a* site are eliminated by the $H_2$ reduction. The result unequivocally indicates that $Sr_3Fe_2O_{6.75}$ is topotactically reduced to $Sr_3Fe_2O_6$. The reversible redox cycles between $Sr_3Fe_2O_{6.75}$ and $Sr_3Fe_2O_6$ take place at higher temperature above 773 K. The observation correlates with the topotactic oxygen intake/release ability between $Sr_3Fe_2O_{6.75}$ and $Sr_3Fe_2O_6$. The oxygen storage capacity of $Sr_3Fe_2O_{6.75}$ and its response rate are higher than those of the conventional $Pt/Ce_2Zr_2O_8$ even in the absence of Pt loading. Thus, $Sr_3Fe_2O_{7-\delta}$ must be of great promise as novel oxygen storage materials.

## Introduction

Transition metal oxides bearing perovskite structure have received much attention, because of their usefulness as the advanced materials such as catalysts, electronic and/or magnetic devices, and oxygen storage materials (OSMs).[1-4] In such application, the characteristic of OSM is in the ability for controlling oxygen partial pressure in gas phase. This ability is not only utilized as the function of oxygen separator or oxygen sensor,[5,6] but also serves as the environmental-related material for purifying pollutant gases emitted from automobiles.[7-13] The automobile exhaust gas contains some pollutant materials such as hydrocarbon (HC), CO and $NO_x$, which are converted into $CO_2$, $H_2O$, and $N_2$ by the automobile three-way catalysts (TWCs).[14,15] The purification efficiency depends on air-to-fuel ratio (A/F), and all pollutant materials are usually purified in a stoichiometric condition of around A/F = 14.7. In low A/F ratios, HC and CO cannot be completely oxidized, whereas in high A/F ratios the reduction of NO to $N_2$ becomes difficult. Needless to say, the adjustment of A/F at the surface of TWCs is responsible for the ability of OSMs.

In the process of purifying automotive exhaust pollutants, the OSM set at a high temperature around 1273 K,[11] and at low A/F conditions (A/F < 14.7) it is further exposed under a reduction condition. A high structural stability under a severe condition is thus undoubtedly one of important functions as OSMs. Various perovskite-related materials or oxysurfide such as $BaYMn_2O_{5+d}$[16,17] or $Pr_2O_2SO_4$[18-20] have been recently reported to exhibit high performance as OSM;[3,21,22] however, much concern have not paid toward their structural stability under severe conditions. If a structural collapse such as phase segregation or decomposition of these compounds is induced by severe conditions, the performance as OSM must be drastically decreased. Accordingly, it is highly required to search and prepare new OSMs having higher structural stability under severe conditions.

$CeO_2$-$ZrO_2$ solid solution is widely used as one of fundamental components in TWCs. Note that the structural framework in $CeO_2$-$ZrO_2$ is substantially maintained in severe conditions.[23] Furthermore, a recent study on the structural and compositional change of pyrochlore-type $CeO_2$-$ZrO_2$ solid solution in the oxidation/reduction process has indicated that the oxidation from $Ce_2Zr_2O_7$ to $Ce_2Zr_2O_8$ systematically lowers the symmetry from *Fd*-3*m* to $P2_13$. In this transformation, the original pyrochlore-type cation ordering is maintained without any intermixing between Ce and Zr atoms.[24] Such a crystallographic transformation is referred to "topotactic transition" has not been explicitly evaluated as one of important abilities in the field of catalyst design for various catalytic reactions such as NO decomposition or combustion reaction of hydrocarbon.

The topotactic transition has been also known to occur in a specific reduction of Sr-Fe mixed oxides bearing perovskite structure.[4,25] For example, the reduction of $Sr^{2+}Fe^{4+}O_3$ with $CaH_2$ yields $Sr^{2+}Fe^{2+}O_2$, the framework of which is analogous

[a] *Department of Molecular Engineering, Graduate School of Engineering, Kyoto University, Kyotodaigaku Katsura, Nishikyo-ku, Kyoto 615-8510, Japan. E-mail: hosokawa@moleng.kyoto-u.ac.jp and tanakat@moleng.kyoto-u.ac.jp*
[b] *Elements Strategy Initiative for Catalysts & Batteries (ESICB), Kyoto University, Kyotodaigaku Katsura, Nishikyo-ku, Kyoto 615-8520, Japan.*
[c] *Precursory Research for Embryonic Science and Technology (PRESTO), Japan Science and Technology Agency (JST), 4-1-8 Honcho, Kawaguchi, Saitama 332-0012, Japan.*

† Electronic Supplementary Information (ESI) available. See DOI: 10.1039/b000000x/

to that of $SrFeO_3$ having perovskite structure. Although the Sr-Fe mixed oxides are expected to serve as OSMs because of the redox property of iron between $Fe^{4+}$ and $Fe^{2+}$, there has been no report for their properties as OSM. In line with such a context, we have engaged in a systematic investigation for the oxygen storage capacities (OSC) of $SrFeO_{3-x}$ and $Sr_3Fe_2O_{7-y}$ and their structural stability under severe reductive conditions. Described herein is the first demonstration that $Sr_3Fe_2O_{7-y}$ has high structural stability in severe reduction conditions, and also high ability as OSM due to topotactic oxygen intake/release. The present observations must be valuable information not only for OSM, but also for the development of new catalyst based on solid state chemistry.

## Experimental section

**Preparation of Sr-Fe mixed oxides and $Ce_2Zr_2O_8$:** Citric acid (400 mmol) was dissolved into deionized water (180 mL) at 353 K. Then, strontium carbonate (10 mmol) and iron nitrate nonahydrate (10 mmol for $SrFeO_{3-x}$ and 6.67 mmol for $Sr_3Fe_2O_{7-y}$) were added and stirred for 2 h to obtain the solution containing metal oxide complexes. Ethylene glycol (400 mmol) was added to this solution, and thus-obtained solution was stirred at 403 K for 4 h to form a gelatinous solution. After the gel was heated in a mantle heater at 623 K for 3 h, the thus-obtained brown powder was calcined at the 1273 K and held at that temperature for 30 min. $Ce_2Zr_2O_8$ was synthesized by the same method as above, and cerium nitrate and zirconium oxynitrate were used as the starting materials.

**Preparation of $Pt/Sr_3Fe_2O_{7-y}$ and $Pt/Ce_2Zr_2O_8$ solid solution:** $Sr_3Fe_2O_{7-y}$ or $Ce_2Zr_2O_8$ was added to an aqueous solution containing a desired amount of $Pt(NO_3)_2(NH_3)_2$, and the slurry was dried on a 80 ºC water bath, followed by calcination in air at 773 K for 5 h. The Pt loading amount was 1 wt% on a metal basis.

**$H_2$-TPR and OSC measurements:** Temperature programed reduction ($H_2$-TPR) with hydrogen was carried out with a flow-type reactor. Hydrogen (2 vol % in Ar; 30 ml $min^{-1}$) was passed through the reactor charged with a sample (0.05 g) under atmospheric pressure. The reactor was heated with an electric furnace with a heating rate of 5 K $min^{-1}$ up to 1223 K, and the amount of $H_2$ consumed was monitored with a TC detector of a Shimadzu GC8A gas chromatograph. The samples reduced in the equipment with $H_2$-TPR were designated as $Sr_3Fe_2O_{7-y}$(red). The abbreviation is followed by reduction temperature. For example, $Sr_3Fe_2O_{7-y}$(red-773) refers to the product obtained by the reduction at 773 K of $Sr_3Fe_2O_{7-y}$.

Oxygen storage capacity measurement (OSC measurement) was carried out with a thermogravimeter (Rigaku Thermoplus). The samples (0.1 g) were heated to 773 K in Ar and held until the constant weights were achieved. Then, weight changes of the samples upon switching the atmosphere every 20 min between 5% $O_2$/Ar and 5% $H_2$/Ar were recorded isothermally to investigate the oxygen intake/release processes.

**Characterizations:** The X-ray powder diffraction patterns (Rigaku multiflex or Rigaku UltimaIV) were recorded using CuKα radiation. For Rietveld analysis, the XRD pattern was recorded on another diffractometer, Rigaku multiflex, and analysed by a RIETAN-FP program.[26] The split pseudo-voigh function of Toraya was used. We optimized the parameters according to the following orders: the unit cell parameter, the fractional coordinate of oxygen and cations and the occupancy of oxygen ions. X-ray absorption fine structure (XAFS) at Fe K-edge or Sr K-edge was measured at the beam line BL01B1 of SPring-8. The XAFS spectra was recorded in a transmittance mode at room temperature, using Si(111) and Si(311) double crystal monochrometers for the measurements at Fe K-edge and Sr K-edge, respectively.

## Results and discussion

The X-ray powder diffraction (XRD) patterns (Fig. 1; a in (A) and c in (B)) of $SrFeO_{3-x}$ and $Sr_3Fe_2O_{7-y}$ synthesized by a Pechini method showed that $SrFeO_{3-x}$ had the space group of *I4/mmm* in the charged ratio of Sr/Fe = 1. The Rietveld analysis (Fig. S1) indicated the existence of an oxygen vacancy site, and the chemical formulation of $SrFeO_{3-x}$ could be determined to be $SrFeO_{2.84}$. When the charged ratio of Sr/Fe was 3/2, phase-pure $Sr_3Fe_2O_{7-y}$ with layered perovskite structure was formed. The oxygen vacancy of $Sr_3Fe_2O_{7-y}$ was the same as that of $SrFeO_{3-x}$ (Fig. S2), and the chemical formulation of $Sr_3Fe_2O_{7-y}$ was determined to be $Sr_3Fe_2O_{6.75}$. The profiles obtained from temperature programed reduction of $SrFeO_{3-x}$ and $Sr_3Fe_2O_{7-y}$ with hydrogen ($H_2$-TPR) are shown in Fig. 2. Two reduction peaks at 750 K and above 850 K were observed in $SrFeO_{3-x}$, but the reduction peak was not clearly observed at above 850 K in $Sr_3Fe_2O_{7-y}$. The theoretical hydrogen consumption can be calculated by the following equations, in which all of the $Fe^{4+}$

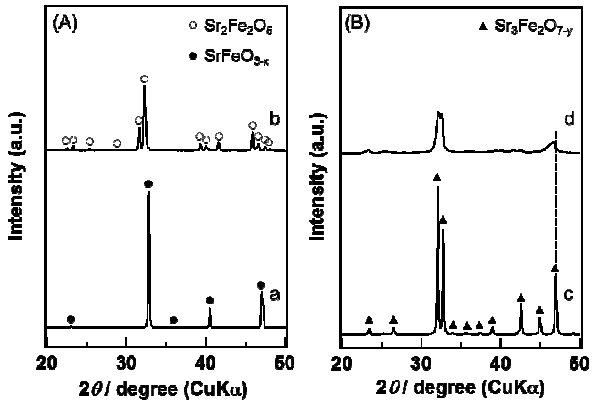


**Fig. 1.** XRD patterns of $SrFeO_{3-x}$ (A) and $Sr_3Fe_2O_{7-y}$ (B). **a** and **c**, as-synthesized sample; **b** and **d**, the sample reduced at 773 K.

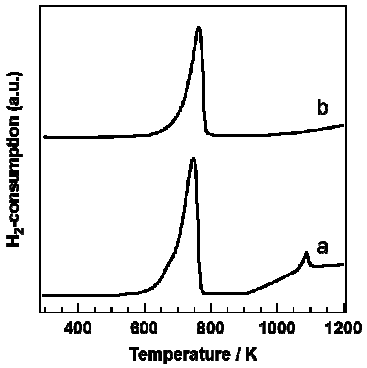


**Fig. 2.** TPR profiles of: **a**, $SrFeO_{3-x}$ and **b**, $Sr_3Fe_2O_{7-y}$.

species are assumed to be reduced to $Fe^{3+}$:

$SrFeO_3 + 1/2H_2 \rightarrow SrFeO_{2.5} + 1/2H_2O$ (1)

$Sr_3Fe_2O_7 + H_2 \rightarrow Sr_3Fe_2O_6 + H_2O$ (2)

In $SrFeO_{3-x}$ and $Sr_3Fe_2O_{7-y}$, the amounts of $H_2$ consumed up to 773 K were 852 μmol-$O_2$/g and 618 μmol-$O_2$/g, respectively. These values corresponded to the theoretical values of 900 μmol-$O_2$/g for $SrFeO_{2.84}$ and 704 μmol-$O_2$/g for $Sr_3Fe_2O_{6.75}$. The results confirmed that all $Fe^{4+}$ species in Sr-Fe mixed oxides were reduced to $Fe^{3+}$ species, as given in the above equations. Actually, the existence of phase-pure $Sr_2Fe_2O_5$, that is $SrFeO_{2.5}$ in eq (1), was observed from XRD pattern (Fig. 1; b in (A)) of $SrFeO_{3-x}$(red-773). (as for the abbreviated formulation of such, see the experimental section) The peaks of $Sr_3Fe_2O_{7-y}$(red-773) shifted to lower angle than those of $Sr_3Fe_2O_{7-y}$, and the peak intensity decreased by the reduction (Fig. 1; d in (B)). Unfortunately, the structural change in the reduction of $Sr_3Fe_2O_{7-y}$ up to 773 K could not be determined by XRD patterns. However, the reduction behaviour of this material is shown later by X-ray absorption near edge structure (XANES) spectra for $Sr_3Fe_2O_{7-y}$.

In the XRD pattern of $SrFeO_{3-x}$(red-1223) (Fig. 3(A)), Fe metal, $Sr_2Fe_2O_5$ and $Sr_3Fe_2O_6$ were observed. The reduction peak observed at above 850 K in $SrFeO_{3-x}$ implies that the reduction from $Fe^{3+}$ to $Fe^{2+}$ or Fe metal is occurring. In the case of $Sr_3Fe_2O_{7-y}$(red-1223) (Fig. 3(B)), a small amount of Fe metal was formed together with $Sr_3Fe_2O_6$, but its amount (2 wt%) was much smaller than that (8 wt%) of $SrFeO_{3-x}$(red-1223). These results indicate that $SrFeO_{3-x}$ easily decomposes to Fe metal or $Sr_3Fe_2O_6$ by $H_2$ reduction above 850 K. Of importance here is that the crystal structure of $Sr_3Fe_2O_{7-y}$ is substantially sustained even by the $H_2$ reduction up to 1223 K.

The results of Rietveld analyses of $Sr_3Fe_2O_{7-y}$ and $Sr_3Fe_2O_{7-y}$(red-1223) are shown in Table 1 and Fig. 4. The structural framework of $Sr_3Fe_2O_{7-y}$ was identical with that of $Sr_3Fe_2O_6$, and the space group could be determined to be *I4/mmm* in each sample. The oxygen ions in 8*g* and 4*e* sites were absolutely occupied in $Sr_3Fe_2O_{7-y}$, and 25% of oxygen vacancy was observed in 2*a* site. It is noted that no oxygen ions in 2*a* site exist in $Sr_3Fe_2O_{7-y}$(red-1223). Fe ions in $Sr_3Fe_2O_{7-y}$ were predominantly present in an octahedral environment. The $H_2$ reduction eliminated oxygen ions in 2*a* site, and the coordination state of Fe ions changed from octaheadral environment to pyramidal with pentacoodinated structure. These results prove that the $Sr_3Fe_2O_{7-y}$ is topotactically reduced to $Sr_3Fe_2O_6$ by the $H_2$ reduction at 1223 K.

The XANES spectra of Sr K-edge and Fe K-edge for $Sr_3Fe_2O_{7-y}$ with or without reduction are shown in Figs. 3(C) and (D). The Sr K-edge XANES spectra of $Sr_3Fe_2O_{7-y}$(red-773) indicates that the form of the post edge at 16115 eV was altered by the reduction. The Sr K-edge XANES spectrum of $Sr_3Fe_2O_{7-y}$(red-773) was similar to that of $Sr_3Fe_2O_{7-y}$(red-1223). The feature of Fe K-edge XANES spectra of reduced samples were nearly the same as those of the fresh sample.

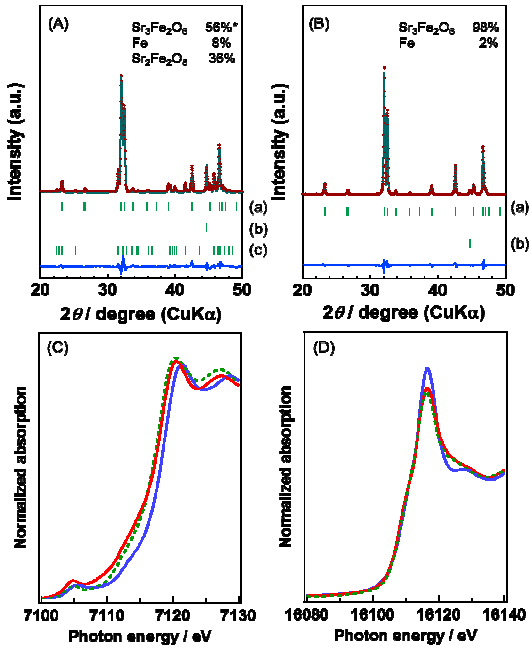


**Fig. 3.** Rietveld analysis of $SrFeO_{3-x}$(red-1223) (A) and $Sr_3Fe_2O_{7-y}$(red-1223) (B). **a**, $Sr_3Fe_2O_6$; **b**, Fe; **c**, $Sr_2Fe_2O_5$. The refinements of $SrFeO_{3-x}$(red-1223) and $Sr_3Fe_2O_{7-y}$(red-1223) led to the residual values of $R_{wp}$ = 15.3% and $R_{wp}$ = 11.7%, respectively.
* The mass fraction (wt%) of the products is shown.
XANES spectra of Fe K-edge (C) and Sr K-edge (D) in $Sr_3Fe_2O_{7-y}$. **Blue line**, $Sr_3Fe_2O_{7-y}$; **dash line**, $Sr_3Fe_2O_{7-y}$(red-773); **red line**, $Sr_3Fe_2O_{7-y}$(red-1223).

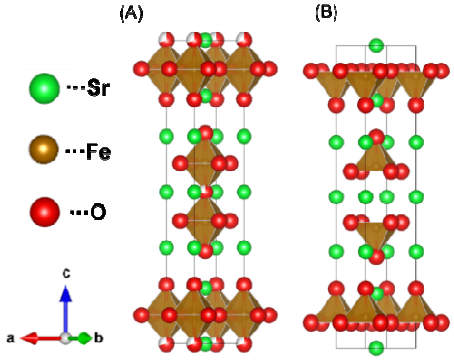


**Fig. 4.** Crystal structures of $Sr_3Fe_2O_{7-y}$ (A) and $Sr_3Fe_2O_{7-y}$(red-1223) (B).

**Table 1**. The results of Rietveld analysis of $Sr_3Fe_2O_{7-y}$ before/after reduction at 1223 K.

| | Site occupancy | | | Lattice parameter | | | $R_{wp}$ |
|---|---|---|---|---|---|---|---|
| | O 8*g* | O 4*e* | O 2*a* | *a*=*b* (Å) | *c* (Å) | *V* (Å$^3$) | (%) |
| $Sr_3Fe_2O_{7-y}$ | 1 | 1 | 0.75(1) | 3.8655(12) | 20.157(6) | 301.20(16) | 11.9 |
| $Sr_3Fe_2O_{7-y}$(red-1223) | 1 | 1 | 0.07(1) | 3.8900(2) | 20.022(1) | 302.98(3) | 11.7 |

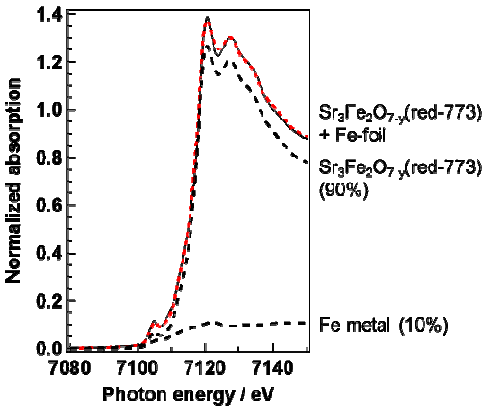


**Fig. 5.** Results of liner curve fitting for Fe K-edge XANES spectra. **Solid line**, $Sr_3Fe_2O_{7-y}$(red-1223); **red line**, spectrum simulated with Fe metal and $Sr_3Fe_2O_{7-y}$(red-773).

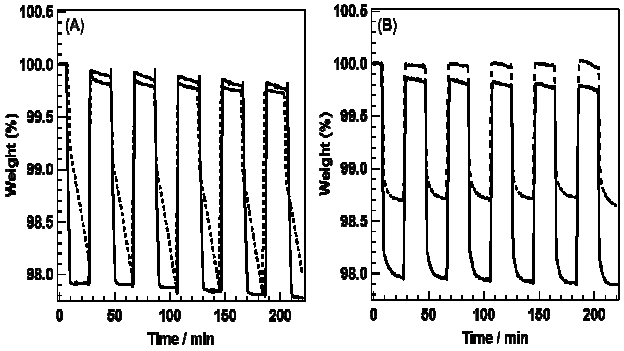


**Fig. 6.** OSC profiles at 773 K of $Sr_3Fe_2O_{7-y}$ (**solid line in (A)**), physically-mixed sample of SrO and α-$Fe_2O_3$(**dash line in (A)**), Pt/$Sr_3Fe_2O_{7-y}$ (**solid line in (B)**) and Pt/$Ce_2Zr_2O_8$ (**dash line in (B)**).

However, the adsorption energy around 7115 eV in reduced samples shifted to lower energy, compared with that of the fresh sample. The edge position has been reported to shift to lower energy with the decrease of Fe valence state.[27] Similarly to this observation, the valence state of Fe decreased by the reduction at 773 K or 1223 K. The Rietveld analysis also indicated that $Sr_3Fe_2O_{6.75}$ was reduced to $Sr_3Fe_2O_6$ at 1223 K. Considering the results, the energy shift can be ascribed to the reduction from $Fe^{3.75+}$ to $Fe^{3+}$.

The XANES spectrum of $Sr_3Fe_2O_{7-y}$(red-773) at around 7110 eV was slightly different from that of $Sr_3Fe_2O_{7-y}$(red-1223). In order to understand the difference, XANES linear curve fitting was performed for $Sr_3Fe_2O_{7-y}$(red-1223) by using Fe metal and $Sr_3Fe_2O_{7-y}$(red-773). A well-simulated spectrum was obtained as shown in Fig. 5. The molar ratios of $Sr_3Fe_2O_{7-y}$(red-773) and Fe metal are 90% and 10%, respectively, the values of which also agreed well with the mass fractions of $Sr_3Fe_2O_6$ and Fe metal derived from Rietveld analysis of $Sr_3Fe_2O_{7-y}$(red-1223). These results allow us to conclude that the local structure around Fe ions in $Sr_3Fe_2O_{7-y}$(red-773) is similar to that in $Sr_3Fe_2O_6$. In addition, the XANES technique indicates that the reduction peak around 750 K observed from $H_2$-TPR profile can be ascribed to the reduction from $Sr_3Fe_2O_{6.75}$ to $Sr_3Fe_2O_6$.

The OSC profiles of $Sr_3Fe_2O_{7-y}$ (Fig. 6) showed that the oxygen intake and release behavior took place at 773 K in response to gas switching of $O_2$ flow and $H_2$ flow. In the oxygen intake/release, the range of weight change, namely OSC, was approximately 2.0 wt%. This value agreed well with the amount of oxygen release estimated from $H_2$-TPR measurement in $Sr_3Fe_2O_{7-y}$ and also from the phase transition between $Sr_3Fe_2O_{6.75}$ and $Sr_3Fe_2O_6$. Although OSC per unit weight of α-$Fe_2O_3$ itself was higher than that of $Sr_3Fe_2O_{7-y}$, the response rate of $Sr_3Fe_2O_{7-y}$ was obviously superior to that of α-$Fe_2O_3$ itself or that of physically-mixed sample of SrO and α-$Fe_2O_3$ (Sr/Fe molar ratio= 3/2) (Table 2 and Fig. S3). The OSC of $Sr_3Fe_2O_{7-y}$ and its response rate were substantially maintained even after the measurement in 5th cycle.

The oxygen intake/release reversibly took place at higher temperature above 773 K, while the OSC slightly decreased with increasing in the operating temperature (Fig. S4). The phenomena was not responsible for a phase segregation or decomposition of $Sr_3Fe_2O_{7-y}$ but rather due to a thermal-desorption of oxygen ions in this oxide, because the weight loss

**Table 2.** Oxygen storage capacities of various samples at 773 K.

| | Rate of oxygen release / storage | | Capacity |
|---|---|---|---|
| | release | storage | ΔW% |
| | μmol-$O_2$/g·s | μmol-$O_2$/g·s | |
| α-$Fe_2O_3$ | 0.63 | 2.82 | 3.4 |
| SrO + α-$Fe_2O_3$ | 2.39 | 5.98 | 1.9 |
| $Sr_3Fe_2O_{7-y}$ | 5.34 | 12.3 | 2.0 |
| Pt/$Sr_3Fe_2O_{7-y}$ | 7.11 | 6.62 | 1.8 |
| Pt/$Ce_2Zr_2O_8$ | 3.99 | 4.38 | 1.3 |

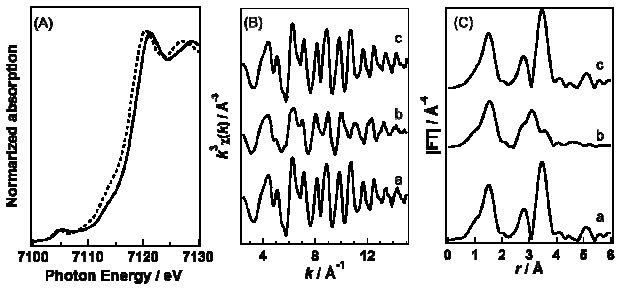


**Fig. 7.** Fe K-edge XANES spectra (A), EXAFS oscillations (B) and Fourier transformed (C) of EXAFS spectra of $Sr_3Fe_2O_{7-y}$ reduced and reoxidized at 773 K in OSC measurement. **Solid line and a**, $Sr_3Fe_2O_{7-y}$; **dash line and b**, the reduced sample; **dot dash line and c**, the reoxidized sample.

above 773 K of $Sr_3Fe_2O_{7-y}$ was observed even in the $O_2$/Ar flow. It is of significance that the reversible redox cycle sustainably proceeds at the operating temperature of the wide range from 773 K to 1073 K.

Figure 7 shows X-ray absorption fine structure (XAFS) spectra of reduced and reoxidized samples of $Sr_3Fe_2O_{7-y}$ in the OSC measurement at 773 K. The XANES and extended X-ray absorption fine structure (EXAFS) spectra of the reduced sample were different from those of the fresh sample. The edge position in XANES spectrum of reduced sample shifted to lower energy than that of the fresh sample, suggesting that $Fe^{4+}$ species in $Sr_3Fe_2O_{7-y}$ was reduced to $Fe^{3+}$ species. The topotactic oxygen release slightly induced the local structural variations around Fe and Sr ions in $Sr_3Fe_2O_{7-y}$ (Fig. 4), resulting

in the change in the EXAFS oscillation and the FT spectrum. Significantly, these spectra of the reoxidized sample are essentially identical with those of the fresh sample. From these results, it is obvious that the redox between $Sr_3Fe_2O_{6.75}$ and $Sr_3Fe_2O_6$ occurred reversibly at 773 K.

Figure S5 shows XRD patterns of the samples obtained by the reduction of physically-mixed sample of SrO and α-$Fe_2O_3$ at 773 K. The peaks assigned as an unknown product may be due to a compound analogous to Sr-Fe mixed oxide. The change in response rate during the reduction process (Fig. 6) is thought to be responsible for the formation of Sr-Fe mixed oxide induced by the redox treatment. On the other hand, since $Fe_3O_4$ (magnetite) was formed by the reduction of α-$Fe_2O_3$ itself, the redox between α-$Fe_2O_3$ and $Fe_3O_4$ mainly occurred. The crystal structure of α-$Fe_2O_3$ was different from that of $Fe_3O_4$.[28,29] The space group of α-$Fe_2O_3$ is *R*-3*c* with corundum structure, the framework of which consists of trigonally distorted octahedra $FeO_6$. The space group of $Fe_3O_4$ is *Fd*-3*m* with inverse spinel structure having octahedra $FeO_6$ and tetrahedra $FeO_4$.[30] The transformation from α-$Fe_2O_3$ to $Fe_3O_4$ was accompanied by elimination of oxygen ions together with rearrangement of Fe ions. In the $H_2$ reduction of $Sr_3Fe_2O_{7-y}$, however, only oxygen ions in 2*a* site were eliminated without rearrangement of Sr and Fe ions (Fig. 4). As mentioned earlier, the response rates for oxygen intake/release of $Sr_3Fe_2O_{7-y}$ were much higher than those of α-$Fe_2O_3$ itself. Therefore, the topotactic oxygen intake/release ability between phase-pure $Sr_3Fe_2O_{6.75}$ and $Sr_3Fe_2O_6$ is apparently related to the fast oxygen storage and release.

The effect of Pt loading is also important in the present study, since the reduction behaviour of $CeO_2$-$ZrO_2$ or $Pr_2O_2SO_4$ has been documented to be significantly improved by Pt or Pd loading.[12, 18–20] Similarly to the observations, TPR profiles of $Sr_3Fe_2O_{6.75}$ with or without Pt loading showed that the peak due to the reduction of $Sr_3Fe_2O_{6.75}$ to $Sr_3Fe_2O_6$ drastically shifted to low temperature of around 450 K by Pt loading (Fig. S6). Thus, Pt loading on $Sr_3Fe_2O_{6.75}$ must exhibit OSC performance below 500 K.

For comparison, the OSC performance of home-made Pt/$Ce_2Zr_2O_8$ was evaluated. The $Ce_2Zr_2O_8$ of home-made sample was comparable to ICSD No. 162778 (Fig. S7), and its OSC was approximately 1.3 wt% (Table 2). This value corresponds to 406 μmol-$O_2$/g-cat and well agrees with the reported value of $CeO_2$-$ZrO_2$ solid solution with 1 wt% Pt.[12] The OSC of $Sr_3Fe_2O_{7-y}$ without Pt loading and its oxygen storage rate were much higher than those of the home-made Pt/$Ce_2Zr_2O_8$. However, the release rate during OSC of $Sr_3Fe_2O_{7-y}$ was not affected by Pt loading, but rather the storage rate drastically decreased (Table 2). Namely, $Sr_3Fe_2O_{7-y}$ surprisingly exhibited high performance, regardless of the presence or absence of Pt loading. These results provide a fruitful perspective that the use of $Sr_3Fe_2O_{7-y}$ for automotive exhaust catalyst could reduce or eliminate the consumption of critical and precious resources such as Pt or Pd.

In comparison with $Ce_2Zr_2O_8$, the merit of $Sr_3Fe_2O_{7-y}$ in OSC is the volume change of unit cell under the redox atmosphere. $Ce_2Zr_2O_8$ has been reported to be transformed into $Ce_2Zr_2O_7$ in a reductive atmosphere.[24] The variation (0.6 %) of the unit cell volume between $Sr_3Fe_2O_{6.75}$ (301.20 Å$^3$) and $Sr_3Fe_2O_6$ (302.98 Å$^3$) was much lower than that (4.1 %) between $Ce_2Zr_2O_8$ (1172.34 Å$^3$) and $Ce_2Zr_2O_7$ (1222.43 Å$^3$). When the variation of unit cell volume is large, the structural defects such as crack or warp are considered to easily take place under redox atmosphere. Therefore, the mechanical strength of $Sr_3Fe_2O_{7-y}$ may be superior to that of $CeO_2$-$ZrO_2$ solid solution.

## Conclusions

In summary, the present study on the reduction-resistances and OSC of $SrFeO_{2.84}$ and $Sr_3Fe_2O_{6.75}$ provides the following unambiguous facts. (1) The $H_2$ reduction of $Sr_3Fe_2O_{6.75}$ at 1223 K results in the formation of $Sr_3Fe_2O_6$ with maintaining its structural framework, whereas $SrFeO_{2.84}$ decomposes to $Sr_3Fe_2O_6$ and Fe metal phases. (2) The topotactic oxygen intake/release ability between $Sr_3Fe_2O_{6.75}$ and $Sr_3Fe_2O_6$ reversibly occurs at the operating temperature of the wide range from 773 K to 1073 K. (3) The OSC of $Sr_3Fe_2O_{6.75}$ and its response rate are higher than those of Pt/$Ce_2Zr_2O_8$ even in the absence of Pt loading. These facts indicate that $Sr_3Fe_2O_{7-y}$ has not only high performance of OSC, but also high structural stability under severe reduction conditions such as extremely high temperature. Therefore, the $Sr_3Fe_2O_{7-y}$ must be promising materials as novel OSMs. If $Sr_3Fe_2O_{7-y}$ which contains Fe and Sr could be utilized in place of $CeO_2$-$ZrO_2$ solid solution, it would be profitable in view of resources, because the order of the Clark number is Fe >> Zr ≈ Sr >> Ce. Finally, we would like to add that the concept of topotactic transition will be regarded as one of criteria for the catalyst design in future.

## Acknowledgements

This study was supported by the Program for Element Strategy Initiative for Catalysts & Batteries (ESICB). The XAFS experiments have been performed with the approval of SPring-8 (Proposal No. 2014A1377).

## References

1 H. Hu, R. Cohen, *Nature,* 2000, **403**, 281.
2 Y. Nishihata, J. Mizuki, T. Akano, H. Tanaka, M. Uenishi, M. Kimura, T. Okamoto, N. Hamada, *Nature,* 2002, **418**, 164.
3 T. Motohashi, Y. Hirano, Y. Masubuchi, K. Oshima, T. Setoyama, S. Kikkawa, *Chem. Mater.,* 2013, **25**, 372.
4 Y, Tsujimoto, C. Tassel, N. Hayashi, T. Watanabe, H. Kageyama, K. Yoshimura, M. Takano, M. Ceretti, C. Ritter, W. Paulus, *Nature,* 2007, **450**, 1062.
5 L. Qiu, T. H. Lee, L. M. Liu, Y. L. Yang, A.J. Jacobson, *Solid State Ionics,* 1995, **76**, 321.
6 A. Thursfield, I. S. Metcalfe, *J. Mater. Chem.,* 2004, **14**, 2475.
7 J. C. Summers, S. A. Ausen, *J. Catal.,* 1979, **58**, 131.
8 M. Ozawa, M. Kimura, A. Isogai, *J. Alloys Compd*., 1993, **193**, 73.
9 J. Kašper, P. Fornasiero, M. Graziani, *Catal. Today,* 1999, **50**, 285.
10 M. Borao, C. D. Leitenburg, G. Dolcetti, A. Travarelli, *J. Catal.,* 2000, **193**, 338.
11 J. Kašper, P. Fornasiero, N. Hickey, *Catal. Today,* 2003, **77**, 419.
12 M. Sugiura, M. Ozawa, A. Suda, T. Suzuki, T. Kanzawa, *Bull. Chem. Soc. Jpn.,* 2005, **78**, 752.
13 R. D. Monte, J. Kašper, *J. Mater. Chem.,* 2005, **15**, 633.
14 J. H. Jones, J. T. Kummer, K. Otto, M. Shelef, E. E. Weaver, *Environmental Sci. Tech.,* 1971, **5**, 790.
15 J. T. Kummer, *Prog. Energy Combust. Sci.,* 1980, **6**, 177.
16 T. Motohashi, T. Ueda, Y. Masubuchi, M. Takiguchi, T. Setoyama, K. Oshima, S. Kikkawa, *Chem. Mater.,* 2010, **22**, 3192.
17 T. Motohashi, T. Ueda, Y. Masubuchi, S. Kikkawa, *J. Ceram. Soc. Jpn.,* 2011, **119**, 894.

18 M. Machida, K. Kawamura, K. Ito, K. Ikeue, *Chem. Mater.,* 2005, **17**, 1487.
19 M. Machida, K. Kawamura, T. Kawano, D. Zhang, K. Inoue, *J. Mater. Chem.*, 2006, **16**, 3084.
20 M. Machida, T. Kawano, M. Eto, D. Zhang, K. Inoue, *Chem. Mater.*, 2007, **19**, 954.
21 M. Krappinen, H. Yamauchi, S. Otani, T. Fujita, T. Motohashi, Y. H. Huang, M. Valkeapää, H. Fjellvåg, *Chem. Mater.,* 2006, **18**, 490.
22 M. Hervieu, A.Guesdon, J. Bourgeois, E. Elkaimïm, M. Poienar, F. Damay, J. Rouquette, A. Maignan, C. Martin, *Nature Mater.,* 2014, **13**, 74.
23 C. E. Hori, H. Permana, K. Y. Simon Ng, A. Brenner, K. More, K. M. Rahmoeller, D. Belton, *Appl. Catal., B,* 1998, **16**, 105.
24 S. N. Achary, S. K. Sali, N. K. Kulkarni, P. S. R. Krishna, A. B. Shinde, A. K. Tyagi, *Chem. Mater.,* 2009, **21**, 5848.
25 H. Kageyama, T. watanabe, Y. Tsujimoto, A. Kitada, Y.Sumida, K. Kanamori, K. Yoshimura, N. Hayashi, S. Muranaka, M. Takano, M. Ceretti, C. Ritter, G. Andre, *Angew. Chem. Int. Ed.,* 2008, **47**, 5740.
26 F. Izumi, K. Momma, *Solid State Phenom.,* 2007, **130**, 15.
27 S. H. Choi, B. R. Wood, J. A. Ryder, A. T. Bell, *J. Phys. Chem. B,* 2003, **107**, 11843.
28 A. H. Hill, F. Jiao, P. G. Bruce, A. Harrison, W. Kockelmann, C. Ritter, *Chem. Mater.,* 2008, **20**, 4891.
29 D. Levy, R. Giustetto, A. Hoser, *Phys. Chem. Minerals,* 2012, **39**, 169.
30 Y. Cudennec, A. Lecerf, *Solid State Sci.,* 2005, **7**, 520.



 

**A graphical and textual abstract**

$Sr_3Fe_2O_{7-\delta}$ has not only high structural stability in severe reduction condition, but also high oxygen storage capacity due to topotactic oxygen intake/release.